Fuel 218 (2018) 350–356

Contents lists available at ScienceDirect

Fuel

journal homepage: www.elsevier.com/locate/fuel

Full Length Article

Velocity profiles of avalanches during hopper discharge

Ningsheng Wang, Jianliang Xu, Xiaolei Guo, Haifeng Lu, Hui Zhao, Weifeng Li, Haifeng Liu*

Key Laboratory of Coal Gasification and Energy Chemical Engineering of Ministry of Education, East China University of Science and Technology, P.O. Box 272, Shanghai 200237, PR China

Shanghai Engineering Research Center of Coal Gasification, East China University of Science and Technology, P.O. Box 272, Shanghai 200237, PR China

GRAPHICAL ABSTRACT

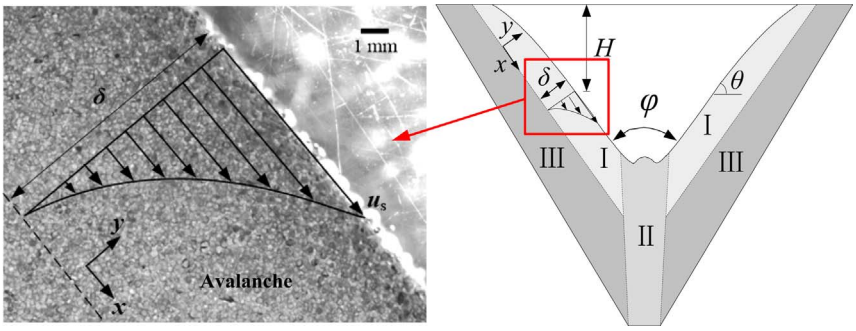

ARTICLE INFO

Keywords:
Avalanche
Discharge
Velocity profile
Viscosity

ABSTRACT

In this paper, we investigate avalanches during the fully developed stage of the discharge in a quasi-two-dimensional wedge-shaped hopper. The velocity profiles of the avalanches are measured by employing a high-speed camera. The velocity profiles vary along the flow, but remain invariant in shape and follow a pure parabolic decrease from the surface. The velocity profiles can be expressed by two parameters of surface velocity and flowing layer thickness. These two parameters increase along the flow, and are both functions of the descending height. Therefore, the velocity profile can be predicted with the descending height. Moreover, a shear-thinning viscosity model is deduced to account for the granular flow behaviour.

1. Introduction

The granular matter is a complicated and unpredictable disordered system. It can not be simply explained by the mechanics of standard solid or liquid. The granular system yields and transforms from a solid state to a liquid state only when the stress exceeds a critical value [1–5]. The study of granular flows has attracted great interest from physicists and engineers due to their ubiquitous applications in numerous natural and industrial situations, such as dunes migration, snow avalanches, and powder handling.

One of the oldest and most important cases of granular flow is the discharge of particles through an orifice. Continuous efforts have been dedicated to understand different features presented by this type of flow, such as free-fall arch [6,7], clogging [7–15], density fluctuations [16,17], segregation [18] and collapse of silos [19] during discharge. Effects of the particle properties [20], gas drag [17,21–25], geometry [10,26–30], and inserts (obstacles) [9,31,32] on the flow behaviour in the silo have also been extensively studied to optimize the design and operation of the hopper.

The velocity field in a hopper is a fundamental indicator of

* Corresponding author at: Key Laboratory of Coal Gasification and Energy Chemical Engineering of Ministry of Education, East China University of Science and Technology, P.O. Box 272, Shanghai 200237, PR China.
E-mail address: hfliu@ecust.edu.cn (H. Liu).

https://doi.org/10.1016/j.fuel.2018.01.053
Received 1 November 2017; Received in revised form 13 December 2017; Accepted 13 January 2018
Available online 20 January 2018
0016-2361/

discharge dynamics. Therefore, many experiments [7,29,33–38] and numerical simulations [16,39–41] have been carried out to obtain the whole velocity field. The digital particle image velocimetry methodology is usually used to obtain the flow field in the discharge experiments [29,33–37,42]. The flow in the hopper is usually distinguished into two types: mass flow, where all the particles are in motion, and funnel flow, where flow takes place only in a central region surrounded by stagnant particles. In funnel flow, a "V" shape crater usually forms at the surface of granular bed, and avalanches occur at the surface of the crater. Albaraki and Antony [29] studied the effect of the internal angle of the hopper on the flow pattern, and presented the mean velocity vector of grains inside the hoppers for both mass flow and funnel flow, but no expression of the velocity field is obtained. Avalanches, which are also called the surface flows and are usually studied on a heap [4,43–47] or in the rotating drum [2,48–52], can also be observed in the late period of the funnel flow for large internal angle. Maiti et al. [33] investigated the granular discharge in eccentric silos and mainly focused on the velocity profiles in the flow region above the orifice. Ferrari and Poletto [42] measured the particle velocity field near the outlet in an aerated hopper, and found that when the aeration rate increases to a certain extent, the initial static particles begin to flow. In the study of dynamical arching with photoelastic particles, the average velocity field is described using a combination of harmonic angular functions and a power law of radial position [7]. In a recent simulation of the mass flow in a conical hopper, the velocity profile is also a power law function of the distance from the orifice but with a different exponent and expression [39].

So far, a number of studies have been performed to investigate the hopper discharge, and studies of the velocity field in the hopper mainly focus on the mass flow and the central region above the orifice in a funnel flow. Detailed expressions for predicting the velocity field in the hopper especially in the avalanches of a funnel flow are still lacking. Here in this paper, we conduct a funnel flow in a quasi-two-dimensional wedge-shaped hopper, and investigate avalanches during the discharge. Moreover, velocity profile for predicting the surface flow are obtained, and a viscosity model is also deduced.

2. Experimental

The experimental setup is simple in its principle, as sketched in Fig. 1, consisting of a high-speed digital camera (Fastcam SA2 by Photron Limited), a digital scale and a quasi-two-dimensional wedge-shaped hopper with an open angle of 60°. We use glass beads of density $\rho_p = 2490\ kg/m^3$ and of particle size $d_p = 131\ \mu m$ and $237\ \mu m$. The cumulative particle size distributions of the glass beads are shown in Fig. 2. Both particle sizes ensure a good flowability of the material. The vertical sidewalls of the hopper are made of two transparent glass plates to allow visualization. The gap between the two sidewalls is $w = 4.5\ mm$ making the front and rear boundaries close enough to achieve a quasi-two-dimensional condition. The flow rates calculated from the measured particle velocities at the outlet match well with the measured flow rates with discrepancies within 8.3%. Therefore, the wall friction in the following is neglect [53,54]. The vertical height of the hopper is 275.0 mm and the width of the outlet is 30.0 mm. The hopper is initially fulfilled with glass beads, and a slide lock is employed at the outlet to control the onset of the discharge.

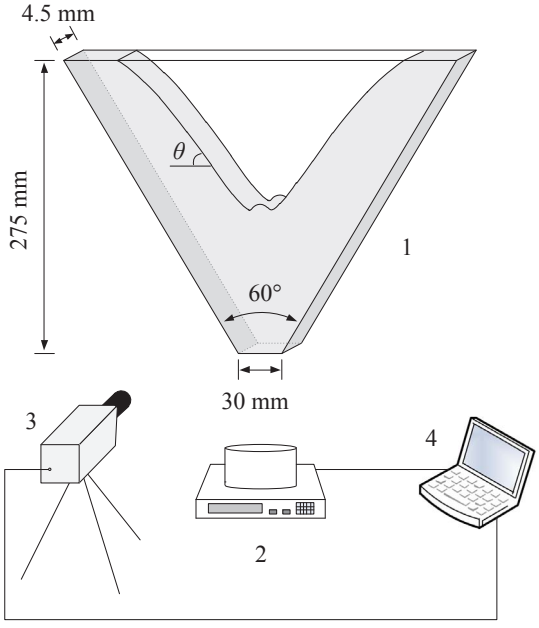

Fig. 1. Sketch of the experimental setup. 1-two dimensional wedge-shaped hopper, 2-digital scale, 3-high-speed digital camera, 4-computer.

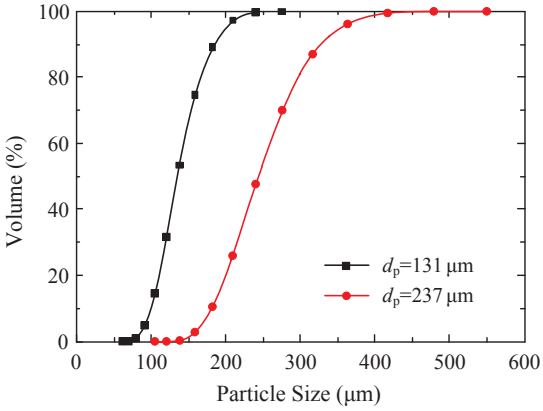

Fig. 2. The cumulative particle size distributions of the glass beads.

The mass flow rates of the glass beads recorded by the digital scale are constant during the discharge, and are highly reproducible from run to run. The mass flow rates are 95.5 g/s and 107.4 g/s for particle size $d_p = 131$ and $237\ \mu m$, respectively. A funnel flow is observed during the discharge, and the granular bed is distinguished into three flow regions (see Fig. 3): downslope flowing layer I, central flow II, and stagnant zone III. The discharge begins with a rapid upward propagation of the central flow region, and once the central flow region reaches the upper surface, the initially horizontal surface becomes concave, and a "V" shape crater is therefore developed at the surface. The evolution of the crater angle φ (defined as the angle between the steepest tangents to the flow surfaces) is shown in Fig. 4. The crater angle φ decreases dramatically in the first second, and then attains a plateau. This can be explained as follow: During the emptying period, the discharge rate is constant, which indicates a constant area variation rate of the crater. Therefore, in the early stage when the crater is small, the combination of increases in both the crater size and the avalanche angle θ (the angle

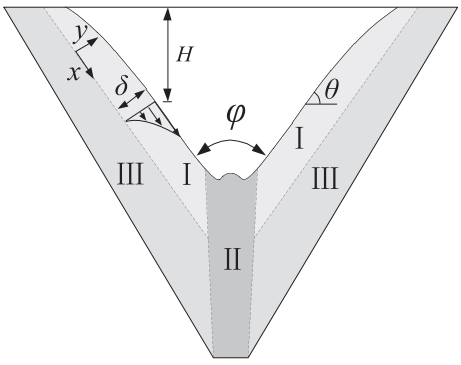

Fig. 3. Schematic of the granular flow in the hopper.

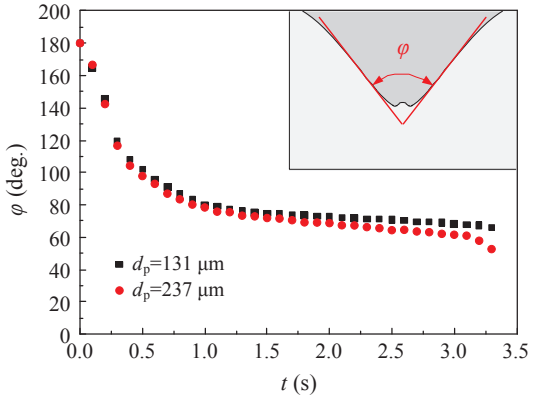

Fig. 4. Evolution of the crater angle φ during the discharge. Inset: definition of the crater angle.

of the inclined flowing layer with respect to the horizontal) is the most efficient and prompt way, which corresponds to the dramatical decrease of the crater angle in Fig. 4. When the crater develops to a certain extent, the increase merely in crater size can already satisfy the requirement of constant area variation rate, and the crater angle is then kept relatively steady, which corresponds to the plateau. For $t > 2.5$ s, the periphery of the crater reaches the inclined sidewalls. Therefore the velocity profiles presented in the following are all measured in the avalanches at successive times (t = 1.1, 1.5, 1.9 and 2.3 s) during the crater-angle-steady duration.

Zoomed images (windows of approximately 20 mm long) of the flowing layer are taken along the flow by the high-speed digital camera from the side. The sampling rate is 1600 images per second, and the resolution is 1536 × 1536 pixels allowing resolving spatial variations of the velocity profile down to the pixel size. The bottom boundary of the avalanche is defined to be the locus of points where the particle velocity decreases down to 1% of the surface velocity. The flowing layer is then defined as the region between the surface and the bottom boundary of the avalanche, as shown in Fig. 3. The flowing layer thickness δ is defined as the distance between the surface and the bottom boundary. The (x, y) axes are defined as follow: x is the direction along the flow, and y is perpendicular to the boundary with the origin set on the bottom boundary.

3. Results and discussion

3.1. Velocity profiles of the avalanches

A typical velocity profile for glass beads of d_p = 237 μm is displayed superimposed to the pile image in Fig. 5, and the dash line represents the bottom boundary of the flowing layer. Figs. 6 and 7 display temporal and spatial evolutions of the velocity profiles of the avalanches during the crater-angle-steady duration, and H denotes the descending height (the vertical distance to the upper initial material level, as shown in Fig. 3).

We can see from Figs. 6 and 7 that the velocity u decreases from a certain value at the surface to zero at the bottom, and the velocity profiles along the flow remain almost invariant in shape. With the same particle size and descending height H, velocity profiles keep almost consistent with each other at different instants (t = 1.1, 1.5, 1.9 and 2.3 s). Thus the velocity profiles of the avalanches during the crater-angle-steady duration are considered to be time-invariant. When rescaled by the surface velocity u_s (measured at the surface of the flowing layer) and the flowing layer thickness δ, as seen in Fig. 8, the velocity profiles collapse well onto a single curve, which can be expressed in a simple parabolic form as

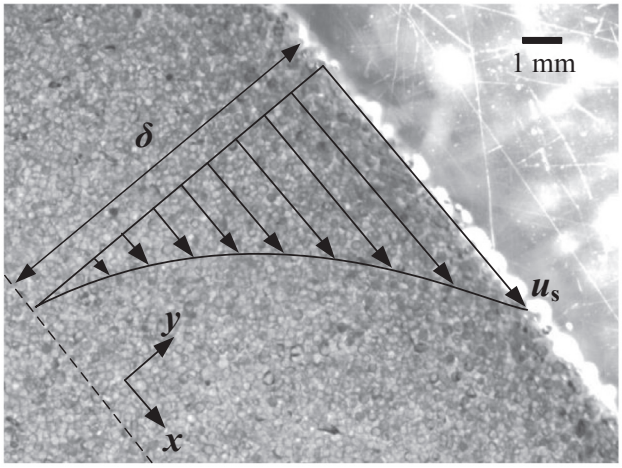

Fig. 5. Typical image of granular flowing layer and the velocity profile superimposed to the image for d_p = 237 μm.

$$\frac{u}{u_s} = \left(\frac{y}{\delta}\right)^2, \tag{1}$$

with correlation coefficient of approximately 0.98. Moving u_s in Eq. (1) to the right-hand side, the velocity profiles can thus be rewritten as

$$u = u_s\left(\frac{y}{\delta}\right)^2, \tag{2}$$

which is different from those observed exponential velocity profiles [45–47], and no linear part is observed.

3.2. Experimental results of the relations between u_s, δ and H

As the particles flow downslope (with increasing H), both the surface velocity and the flowing layer thickness increase (see Figs. 6 and 7). In other words, particles accelerate along the flow, and erode the stagnant zone urging more particles into motion at the bottom, which results in the increase of the surface velocity and flowing layer thickness. This flow property dramatically contrasts with that of uniform granular flows on a heap [4,43,44], which has a constant velocity profile along the flow.

Fig. 9 displays the plot of dimensionless surface velocity $u_s/\sqrt{gd_p}$ versus dimensionless thickness δ/d_p. We can see that $u_s/\sqrt{gd_p}$ increases linearly with δ/d_p, and all data collapse onto a single curve. The solid line indicates fit to the data with correlation coefficient of approximately 0.98, showing that the dimensionless surface velocity is proportional to the dimensionless thickness,

$$\frac{u_s}{\sqrt{gd_p}} = k\frac{\delta}{d_p}, \tag{3}$$

where k = 0.32 is a constant that independent of the particle size.

Therefore, the ratio of the surface velocity to the flowing-layer thickness can be obtained as

$$\frac{u_s}{\delta} = k\sqrt{\frac{g}{d_p}}, \tag{4}$$

which indicates that the ratio u_s/δ depends only on the particle size and is proportional to $\sqrt{g/d_p}$.

Fig. 10 displays the variations of the surface velocity u_s with the descending height H. We can see that the experimental results for different particle sizes collapse well onto a single curve, and can be fit to a power law as

$$u_s = 2.93\sqrt{H}. \tag{5}$$

This power law indicates a nearly uniformly accelerative motion of

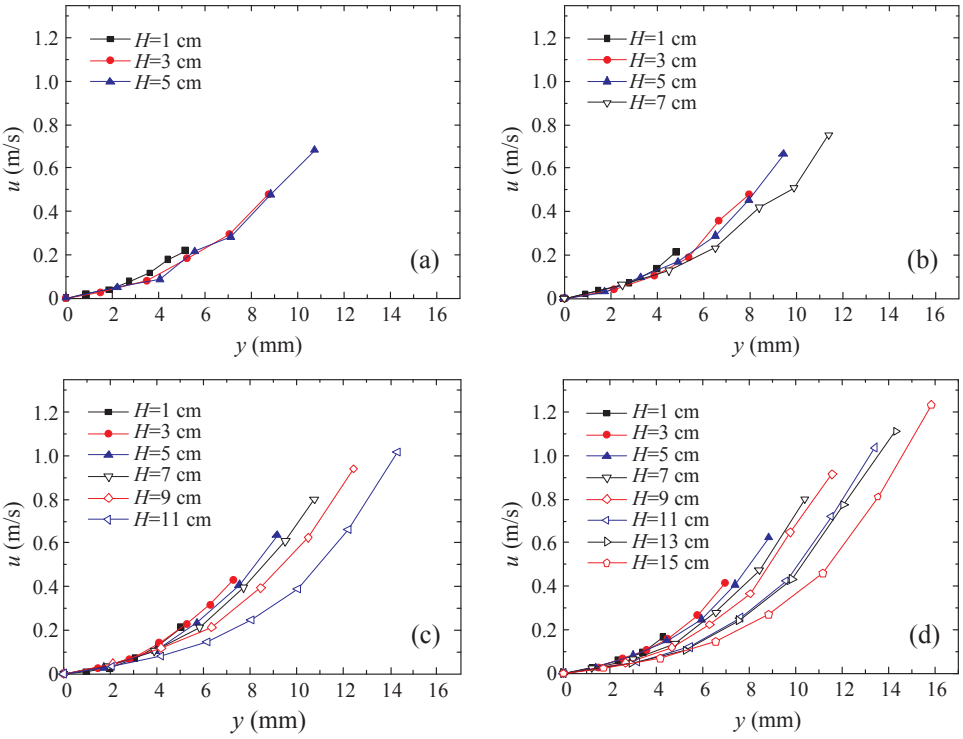

Fig. 6. Temporal and spatial evolutions of velocity profiles for d_p = 237 μm: (a) t = 1.1 s, (b) t = 1.5 s, (c) t = 1.9 s, (d) t = 2.3 s.

the particles at the surface along the flow.

Fig. 11 displays the variations of the flowing layer thickness δ with d_pH, in which the experimental data collapse well onto a single curve. The collapsed data can be fit to a power law with exponent 0.5, yielding

$$\delta = 2.81\sqrt{d_pH}. \quad (6)$$

This power law expression well interprets the curve shape of the flow surface in Fig. 3.

3.3. Theoretical results of the relations between u_s, δ and H

To study the relation between u_s and H, we neglect the contribution of wall friction [53,54], and assume that the inter-particle friction is the dominant drawback force and follows the Coulomb law [44]. The net force along the flow acting on unit mass of the glass beads at the surface is therefore given by $g\sin\theta - \mu g\cos\theta$, where μ is the internal friction coefficient and is the tangent value of the internal friction angle α.

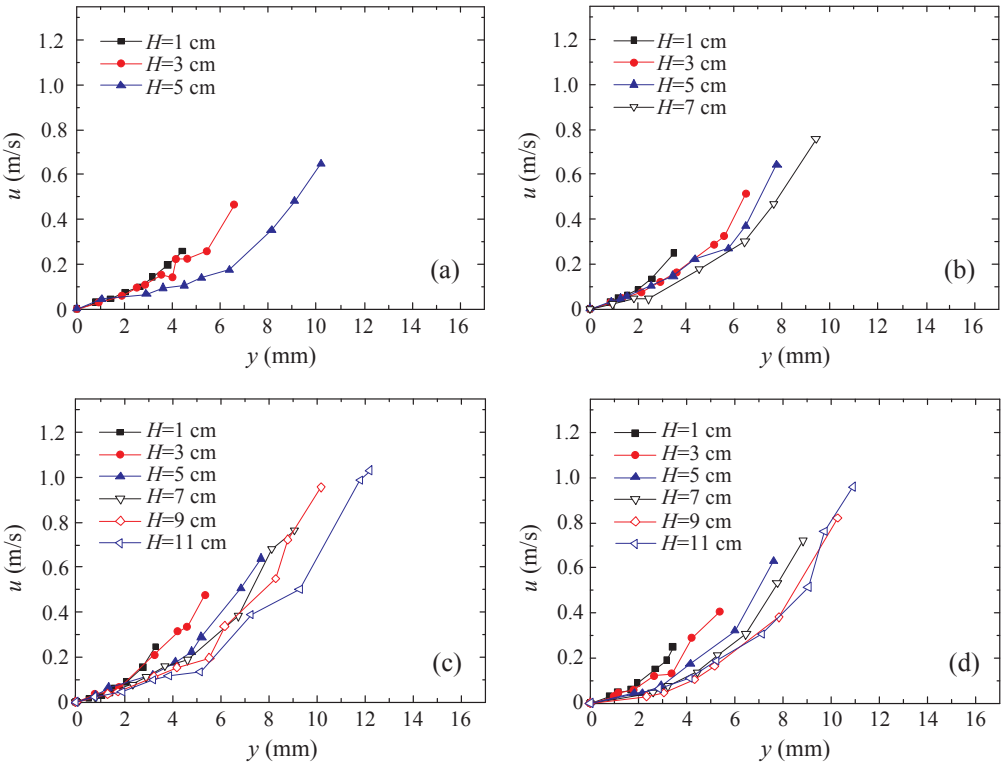

Fig. 7. Temporal and spatial evolutions of velocity profiles for d_p = 131 μm: (a) t = 1.1 s, (b) t = 1.5 s, (c) t = 1.9 s, (d) t = 2.3 s.

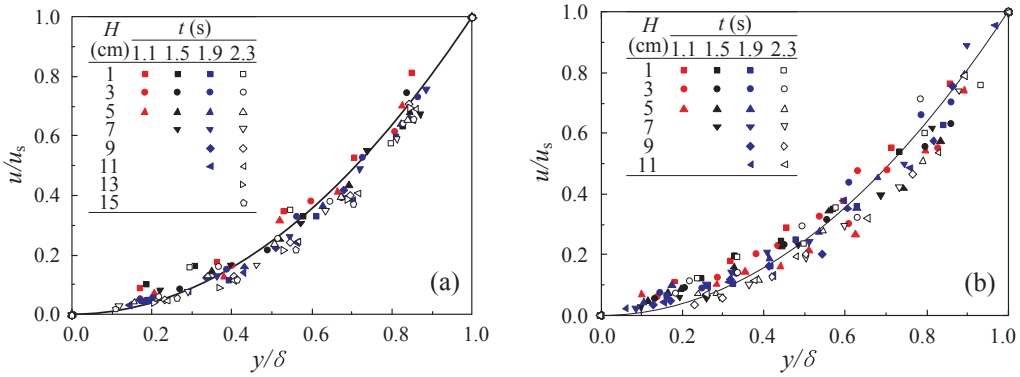

Fig. 8. Rescaled velocity profiles. (a) d_p = 237 μm, (b) d_p = 131 μm. The solid lines are the fits of the rescaled velocity profiles to a power law as $u/u_s = (y/\delta)^2$.

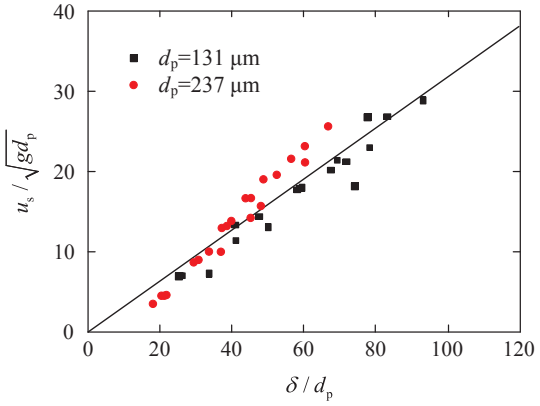

Fig. 9. Plot of dimensionless surface velocity versus dimensionless thickness. The solid line is the linear fit to the data.

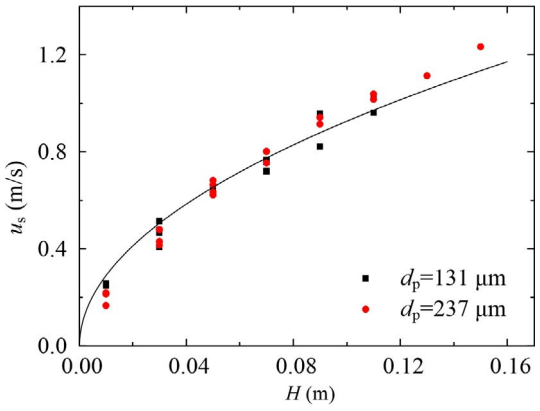

Fig. 10. Variation of u_s with H. The solid line is the fit to a power law between u_s and H.

Moreover, we approximate the free surface as a flat inclined plane, and assume that the particles at the surface move down the inclined plane from the top (zero velocity) with a uniform acceleration. Applying the Newton's second law to unit mass of the glass beads at the surface, we can then obtain that

$$a = g\sin\theta - \mu g\cos\theta = (\sin\theta - \tan\alpha\cos\theta)g, \tag{7}$$

where a is the uniform acceleration in the flow direction. Thus the velocity u_s at the descending height H is given by

$$u_s^2 = 2a\frac{H}{\sin\theta}, \tag{8}$$

where $H/\sin\theta$ is the displacement along the flow from the top. Substituting Eq. (7) into Eq. (8), the expression of surface velocity u_s can be rewritten as

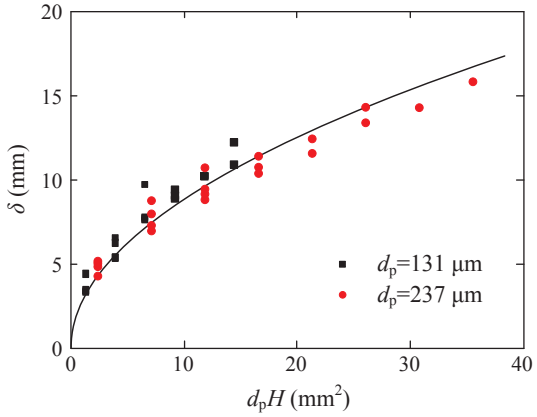

Fig. 11. Variation of δ with H. The solid line is the fit to a power law between δ and H.

$$u_s = \sqrt{2\left(1-\frac{\tan\alpha}{\tan\theta}\right)gH}. \tag{9}$$

Taking g = 9.8 m/s^2, θ = 50.8° and α = 21.3°, we can obtain that

$$u_s = 3.66\sqrt{H}, \tag{10}$$

which is in accord with the experimental result Eq. (5) in form. It is worth noting that the interparticle collisions and the effects of the sidewalls on the granular flows [44,55] are not taken into account in Eq. (7). In this view, it is reasonable for the coefficient 3.66 to be slightly larger than that 2.93 form the experiment, and Eq. (10) is thus considered quite close to equation Eq. (5), further indicating the uniformly accelerative motion of the particles at the surface.

Moreover, substituting Eq. (9) into Eq. (4), the flowing layer thickness δ can be obtained as

$$\delta = \frac{1}{k}\sqrt{2\left(1-\frac{\tan\alpha}{\tan\theta}\right)}\sqrt{d_pH}. \tag{11}$$

It should be noted that Eq. (11) is a semi-empirical correlation and can be predictive only if the coefficient k is provided. Nevertheless, this coefficient could be obtained from a data regression as illustrated in Fig. 9. Further, Eq. (11) is consistent in form with the experimental result in Eq. (6), and yields

$$\delta = 3.65\sqrt{d_pH} \tag{12}$$

when taking θ = 50.8° and α = 21.3°. The coefficient 3.65 in Eq. (12) is considered approximately consistent with experimental results in Eq. (6).

Therefore, the velocity profiles in the flowing layer during the discharge can be predicted by substituting Eqs. (9) and (11) into Eq. (2) as

$$u = k^2\sqrt{\frac{g\tan\theta}{2(\tan\theta-\tan\alpha)d_p^2H}}y^2 \tag{13}$$

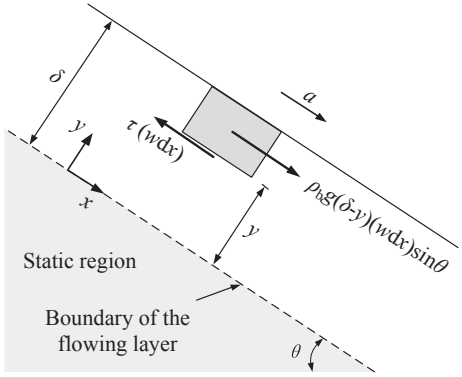

Fig. 12. Force diagram of the control volume.

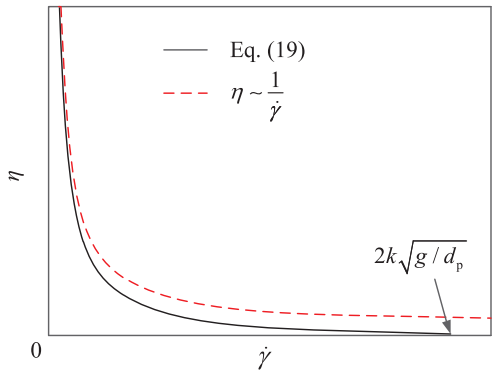

Fig. 13. Plot of the apparent viscosity versus shear rate.

3.4. Apparent viscosity of the avalanches

The shear rate γ, defined as the derivative of the velocity profile, can be derived from Eq. (2) as

$$\dot{\gamma} = \frac{\mathrm{d}u}{\mathrm{d}y} = \frac{2u_s}{\delta^2}y, \tag{14}$$

which shows a linear increase of the shear rate $\dot{\gamma}$ with y at the given cross section. It is worth noting that this parabolic decrease in velocity is quite the opposite of that in a Newtonian fluid flowing on an inclined plane. To the Newtonian fluid with a constant viscosity, the parabolic velocity profile has a null shear rate at the surface and a maximum one at the bottom. Therefore, the rheological behaviour in the granular flow must be different from that in Newtonian fluid.

For the sake of simplicity, we take the granular media as a continuum to study the rheological behaviour. Fig. 12 displays the force diagram of the control volume. The total shear stress τ in the granular flow obeys

$$\tau = \eta\dot{\gamma}, \tag{15}$$

To further simplify the analysis, we neglect the contribution of wall friction [53,54]. Considering that the particles flow downhill with an acceleration of a, the force balance of the granular flow can be written as

$$\rho g(\delta - y)(w\mathrm{d}x)\sin\theta - \tau(w\mathrm{d}x) = \rho a(\delta - y)(w\mathrm{d}x), \tag{16}$$

Substituting Eqs. (14) and (15) into Eq. (16), the apparent viscosity can be deduced as a function of the shear rate

$$\eta = \rho\delta(g\sin\theta - a)\left(\frac{1}{\dot{\gamma}} - \frac{\delta}{2u_s}\right). \tag{17}$$

Substituting Eqs. (4) and (7) into Eq. (17), the apparent viscosity can be further expressed as

$$\eta = \rho g\delta\left(\frac{1}{\dot{\gamma}} - \frac{1}{2k}\sqrt{\frac{d_p}{g}}\right)\tan\alpha\cos\theta. \tag{18}$$

Therefore, the apparent viscosity is proportional to the shear rate term as

$$\eta \sim \frac{1}{\dot{\gamma}} - \frac{1}{2k}\sqrt{\frac{d_p}{g}}, \tag{19}$$

which indicates a shear-thinning rheology of the granular flow.

Fig. 13 displays the apparent viscosity in Eq. (19), and the dashed line indicates $\eta \sim 1/\dot{\gamma}$. We can see that the apparent viscosity diverges to infinity when the shear rate goes to zero, and decreases to zero when the shear rate increase to a certain value. This is in accord with our intuition about the granular that the apparent viscosity is zero at the surface of the granular flow, and when the apparent viscosity increases to infinity, particles stop flowing and remain static.

4. Conclusions

In this paper, avalanches during the fully developed stage of the discharge in a quasi-two-dimensional wedge-shaped hopper have been investigated. The velocity profiles we obtain here vary along the flow, but remain invariant in shape and follow a pure parabolic decrease from the surface. Particles nearly flow downslope with a constant acceleration. The surface velocity u_s is found proportional to the flowing layer thickness δ as $u_s/\delta = k\sqrt{g/d_p}$. The surface velocity u_s and the flowing layer thickness both increase with the descending height H in a power law with exponent 0.5. Finally, a velocity model is deduced to predict velocity profile of the avalanche with the descending height. In addition, a shear-thinning viscosity model is deduced to account for the granular flow by employing the velocity profile.

Acknowledgements

This work was supported by the National Natural Science Foundation of China [U1402272, 21206041]; and the Fundamental Research Funds for the Central Universities.

References

[1] Fenistein D, van Hecke M. Kinematics: wide shear zones in granular bulk flow. Nature (London) 2003;425(6955):256.
[2] du Pont SC, Fischer R, Gondret P, Perrin B, Rabaud M. Instantaneous velocity profiles during granular avalanches. Phys Rev Lett 2005;94(4):048003.
[3] Corwin EI, Jaeger HM, Nagel SR. Structural signature of jamming in granular media. Nature (London) 2005;435(7045):1075–8.
[4] Jop P, Forterre Y, Pouliquen O. A constitutive law for dense granular flows. Nature (London) 2006;441(7094):727–30.
[5] van Hecke M. Granular matter: a tale of tails. Nature (London) 2005;435(7045):1041–2.
[6] Rubio-Largo SM, Janda A, Maza D, Zuriguel I, Hidalgo RC. Disentangling the free-fall arch paradox in silo discharge. Phys Rev Lett 2015;114(23):238002.
[7] Vivanco F, Rica S, Melo F. Dynamical arching in a two dimensional granular flow. Granular Matter 2012;14(5):563–76.
[8] Sheldon HG, Durian DJ. Granular discharge and clogging for tilted hoppers. Granular Matter 2010;12(6):579–85.
[9] Lozano C, Janda A, Garcimartín A, Maza D, Zuriguel I. Flow and clogging in a silo with an obstacle above the orifice. Phys Rev E 2012;86(3):031306.
[10] Thomas CC, Durian DJ. Geometry dependence of the clogging transition in tilted hoppers. Phys Rev E 2013;87(5):052201.
[11] To K. Jamming transition in two-dimensional hoppers and silos. Phys Rev E 2005;71(6):060301.
[12] Tewari S, Dichter M, Chakraborty B. Signatures of incipient jamming in collisional hopper flows. Soft Matter 2013;9(20):5016–24.
[13] To K, Lai P-Y, Pak HK. Jamming of granular flow in a two-dimensional hopper. Phys Rev Lett 2001;86(1):71–4.
[14] Thomas CC, Durian DJ. Fraction of clogging configurations sampled by granular hopper flow. Phys Rev Lett 2015;114(17):178001.
[15] Masuda T, Nishinari K, Schadschneider A. Critical bottleneck size for jamless particle flows in two dimensions. Phys Rev Lett 2014;112(13):138701.
[16] Mollon G, Zhao J. Characterization of fluctuations in granular hopper flow. Granular Matter 2013;15(6):827–40.
[17] Wu X, Måløy K, Hansen A, Ammi M, Bideau D. Why hour glasses tick. Phys Rev Lett

1993;71(9):1363–6.
[18] Ketterhagen WR, Curtis JS, Wassgren CR, Kong A, Narayan PJ, Hancock BC. Granular segregation in discharging cylindrical hoppers: a discrete element and experimental study. Chem Eng Sci 2007;62(22):6423–39.
[19] Gutiérrez G, Colonnello C, Boltenhagen P, et al. Silo collapse under granular discharge. Phys Rev Lett 2015;114(1):018001.
[20] Liu Y, Lu H, Guo X, Gong X, Sun X, Zhao W. An investigation of the effect of particle size on discharge behavior of pulverized coal. Powder Technol 2015;284:47–56.
[21] Hilton JE, Cleary PW. Granular flow during hopper discharge. Phys Rev E 2011;84(1):011307.
[22] Ouwerkerk CED, Molenaar HJ, Frank MJW. Aerated bunker discharge of fine dilating powders. Powder Technol 1992;72(3):241–53.
[23] Nedderman RM, Tūzūn U, Thorpe RB. The effect of interstitial air pressure gradients on the discharge from bins. Powder Technol 1983;35(1):69–81.
[24] Donsi G, Ferrari G, Poletto M, Russo P. Gas pressure measurements inside an aerated hopper. Chem Eng Res Des 2004;82(A1):72–84.
[25] Barletta D, Donsi G, Ferrari G, Poletto M. On the role and the origin of the gas pressure gradient in the discharge of fine solids from hoppers. Chem Eng Sci 2003;58(23–24):5269–78.
[26] Serrano DA, Medina A, Ruiz Chavarria G, Pliego M, Klapp J. Mass flow rate of granular material flowing from tilted bins. Powder Technol 2015;286:438–43.
[27] Medina A, Cabrera D, López-Villa A, Pliego M. Discharge rates of dry granular material from bins with lateral exit holes. Powder Technol 2014;253:270–5.
[28] Maiti R, Das G, Das PK. Experiments on eccentric granular discharge from a quasi-two-dimensional silo. Powder Technol 2016;301:1054–66.
[29] Albaraki S, Antony SJ. How does internal angle of hoppers affect granular flow? Experimental studies using digital particle image velocimetry. Powder Technol 2014;268:253–60.
[30] Kunte A, Doshi P, Orpe AV. Spontaneous jamming and unjamming in a hopper with multiple exit orifices. Phys Rev E 2014;90(2):020201.
[31] Zuriguel I, Janda A, Garcimartín A, Lozano C, Arévalo R, Maza D. Silo clogging reduction by the presence of an obstacle. Phys Rev Lett 2011;107(27):278001.
[32] Alonso-Marroquin F, Azeezullah SI, Galindo-Torres SA, Olsen-Kettle LM. Bottlenecks in granular flow: when does an obstacle increase the flow rate in an hourglass? Phys Rev E 2012;85(2):020301.
[33] Maiti R, Meena S, Das PK, Das G. Flow field during eccentric discharge from quasi-two-dimensional silos–extension of the kinematic model with validation. AIChE J 2016;62(5):1439–53.
[34] Sielamowicz I, Blonski S, Kowalewski TA. Optical technique DPIV in measurements of granular material flows, Part 1 of 3—plane hoppers. Chem Eng Sci 2005;60(2):589–98.
[35] Sielamowicz I, Błoński S, Kowalewski TA. Digital particle image velocimetry (DPIV) technique in measurements of granular material flows, Part 2 of 3-converging hoppers. Chem Eng Sci 2006;61(16):5307–17.
[36] Steingart DA, Evans JW. Measurements of granular flows in two-dimensional hoppers by particle image velocimetry. Part I: experimental method and results. Chem Eng Sci 2005;60(4):1043–51.
[37] Medina A, Córdova JA, Luna E, Treviño C. Velocity field measurements in granular gravity flow in a near 2D silo. Phys Lett A 1998;250(1–3):111–6.
[38] Janda A, Zuriguel I, Maza D. Flow rate of particles through apertures obtained from self-similar density and velocity profiles. Phys Rev Lett 2012;108(24):248001.
[39] Magalhães FGR, Atman APF, Moreira JG, Herrmann HJ. Analysis of the velocity field of granular hopper flow. Granular Matter 2016;18(2):33.
[40] Arévalo R, Garcimartín A, Maza D. Anomalous diffusion in silo drainage. Eur Phys J E 2007;23(2):191–8.
[41] Zheng QJ, Yu AB. Finite element investigation of the flow and stress patterns in conical hopper during discharge. Chem Eng Sci 2015;129:49–57.
[42] Ferrari G, Poletto M. The particle velocity field inside a two-dimensional aerated hopper. Powder Technol 2002;123(2–3):242–53.
[43] Komatsu TS, Inagaki S, Nakagawa N, Nasuno S. Creep motion in a granular pile exhibiting steady surface flow. Phys Rev Lett 2001;86(9):1757–60.
[44] Taberlet N, Richard P, Valance A, et al. Superstable granular heap in a thin channel. Phys Rev Lett 2003;91(26):264301.
[45] Richard P, Valance A, Métayer J-F, et al. Rheology of confined granular flows: scale invariance, glass transition, and friction weakening. Phys Rev Lett 2008;101(24):248002.
[46] Bonamy D, Daviaud F, Laurent L. Experimental study of granular surface flows via a fast camera: a continuous description. Phys Fluids 2002;14(5):1666.
[47] MiDi GDR. On dense granular flows. Eur Phys J E 2004;14(4):341–65.
[48] Socie BA, Umbanhowar P, Lueptow RM, Jain N, Ottino JM. Creeping motion in granular flow. Phys Rev E 2005;71(3):031304.
[49] Alizadeh E, Dubé O, Bertrand F, Chaouki J. Characterization of mixing and size segregation in a rotating drum by a particle tracking method. AIChE J 2013;59(6):1894–905.
[50] Mellmann J, Specht E, Liu X. Prediction of rolling bed motion in rotating cylinders. AIChE J 2004;50(11):2783–93.
[51] Ottino JM, Khakhar DV. Scaling of granular flow processes: from surface flows to design rules. AIChE J 2002;48(10):2157–66.
[52] Rasouli M, Dubé O, Bertrand F, Chaouki J. Investigating the dynamics of cylindrical particles in a rotating drum using multiple radioactive particle tracking. AIChE J 2016;62(8):2622–34.
[53] Orpe AV, Khakhar DV. Solid-fluid transition in a granular shear flow. Phys Rev Lett 2004;93(6):068001.
[54] Orpe AV, Khakhar DV. Scaling relations for granular flow in quasi-two-dimensional rotating cylinders. Phys Rev E 2001;64(3):031302.
[55] Jop P, Forterre Y, Pouliquen O. Crucial role of sidewalls in granular surface flows: consequences for the rheology. J Fluid Mech 2005;541:167–92.